






Tidal Dissipation in WASP-12

Nevin N. Weinberg¹ , Meng Sun², Phil Arras² , and Reed Essick¹ ¹ Department of Physics, and Kavli Institute for Astrophysics and Space Research, Massachusetts Institute of Technology, Cambridge, MA 02139, USA² Department of Astronomy, University of Virginia, P.O. Box 400325, Charlottesville, VA 22904-4325, USA
Received 2017 August 31; revised 2017 September 22; accepted 2017 October 1; published 2017 October 24

Abstract

WASP-12 is a hot Jupiter system with an orbital period of $P = 1.1$ days, making it one of the shortest-period giant planets known. Recent transit timing observations by Maciejewski et al. and Patra et al. found a decreasing period with $P/|\dot{P}| = 3.2$ Myr. This has been interpreted as evidence of either orbital decay due to tidal dissipation or a long-term oscillation of the apparent period due to apsidal precession. Here, we consider the possibility that it is orbital decay. We show that the parameters of the host star are consistent with either a $M_* \simeq 1.3 M_\odot$ main sequence star or a $M_* \simeq 1.2 M_\odot$ subgiant. We find that if the star is on the main sequence, the tidal dissipation is too inefficient to explain the observed \dot{P} . However, if it is a subgiant, the tidal dissipation is significantly enhanced due to nonlinear wave-breaking of the dynamical tide near the star's center. The subgiant models have a tidal quality factor $Q'_* \simeq 2 \times 10^5$ and an orbital decay rate that agrees well with the observed \dot{P} . It would also explain why the planet survived for $\simeq 3$ Gyr while the star was on the main sequence and yet is now inspiraling on a 3 Myr timescale. Although this suggests that we are witnessing the last $\sim 0.1\%$ of the planet's life, the probability of such a detection is a few percent given the observed sample of $\simeq 30$ hot Jupiters in $P < 3$ -day orbits around $M_* > 1.2 M_\odot$ hosts.

Key words: binaries: close – planet–star interactions – planets and satellites: individual (WASP-12b) – stars: oscillations

1. Introduction

The orbits of hot Jupiters are expected to decay due to tidal dissipation within their host stars (Rasio et al. 1996). While there is considerable indirect evidence of orbital decay in the ensemble properties of hot Jupiter systems (Jackson et al. 2008, 2009; Hansen 2010; Penev et al. 2012; Schlaufman & Winn 2013; Teitler & Königl 2014), the recent transit timing observations of WASP-12 by Maciejewski et al. (2016) and Patra et al. (2017) could be the first direct evidence of the orbital decay of an individual system. They detect a decrease in the orbital period at a rate $\dot{P} = -29 \pm 3$ ms yr⁻¹. This corresponds to an inspiral timescale of just $P/|\dot{P}| = 3.2$ Myr and a stellar tidal quality factor $Q'_* \approx 2 \times 10^5$.

As both studies note, it is difficult to tell whether the observed \dot{P} is due to orbital decay or is instead a portion of a long-term (≈ 14 yr) oscillation of the apparent period. The latter could be due to apsidal precession if the eccentricity is $e \approx 0.002$. However, it is not clear how to maintain such an e in the face of rapid tidal circularization. Patra et al. (2017) mention gravitational perturbations from the star's convective eddies, a mechanism Phinney (1992) proposed to explain the small but nonzero eccentricities of pulsars orbiting white dwarfs. However, the host star ($M_* \simeq 1.3 M_\odot$) has a very low-mass convective envelope ($\simeq 10^{-3} M_\odot$) and we estimate that there is too little energy in the eddies to maintain an $e \sim 10^{-3}$. Another mechanism that can cause decade-long oscillations of the period that Patra et al. mention is the Applegate (1992) effect, which invokes variations in the quadrupole moment of the star over a magnetic activity cycle. However, Watson & Marsh (2010) estimate that for WASP-12b, this effect shifts the transit arrival times by $\Delta T \lesssim 10$ s after $T \approx 10$ yr. This corresponds to an average $|\dot{P}| \simeq 2P\Delta T/T^2 < 1$ ms yr⁻¹ (Birkby et al. 2014), more than an order of magnitude smaller than the measured value.

With a few more years of monitoring it should be possible to distinguish unequivocally between orbital decay and precession (Patra et al. 2017). In this paper, we consider whether the decay explanation is plausible. In Section 2, we construct stellar models that fit the observed properties of WASP-12. In Section 3, we describe the relevant tidal processes and then use the stellar models to calculate the expected rate of tidal dissipation. We conclude in Section 4.

2. Stellar Models of WASP-12

The WASP-12 host star has an effective temperature $T_{\text{eff}} = 6300 \pm 150$ K and a mean density $\rho_* \equiv 3M_*/4\pi R_*^3 = 0.475 \pm 0.038$ g cm⁻³ (Hebb et al. 2009; Chan et al. 2011; here and below we adopt the values from the latter reference). Note that ρ_* is measured solely from the transit parameters of the light curve (see Seager & Mallén-Ornelas 2003) and is not derived from a fit to stellar evolution models, unlike the stellar mass M_* and radius R_* . The spectrum of WASP-12 is consistent with a supersolar metallicity ($[\text{Fe}/\text{H}] = 0.30 \pm 0.10$) and a spin that is slow ($v \sin i < 2.2 \pm 1.5$ km s⁻¹) and likely misaligned with the planet's orbital plane (Schlaufman 2010; Albrecht et al. 2012). By fitting stellar models to T_{eff} , ρ_* , and the metallicity, Chan et al. (2011; see also Hebb et al. 2009; Enoch et al. 2010; Fossati et al. 2010; Maciejewski et al. 2011) find $M_* = 1.36 \pm 0.14 M_\odot$, $R_* = 1.595 \pm 0.071 R_\odot$, and a surface gravity $\log g_* = 4.164 \pm 0.029$ (in cgs units). Based on three separate age-dating techniques (lithium abundance, isochrone analysis, and gyrochronology) Hebb et al. (2009) find that WASP-12 is likely to be several Gyr old, implying an age comparable to its main sequence lifetime.

We construct stellar models using the MESA stellar evolution code (Paxton et al. 2011, 2013, 2015), version 9575. We assume a solar abundance scale based on Asplund et al. (2009; solar metallicity $Z = Z_\odot = 0.0142$) and follow the

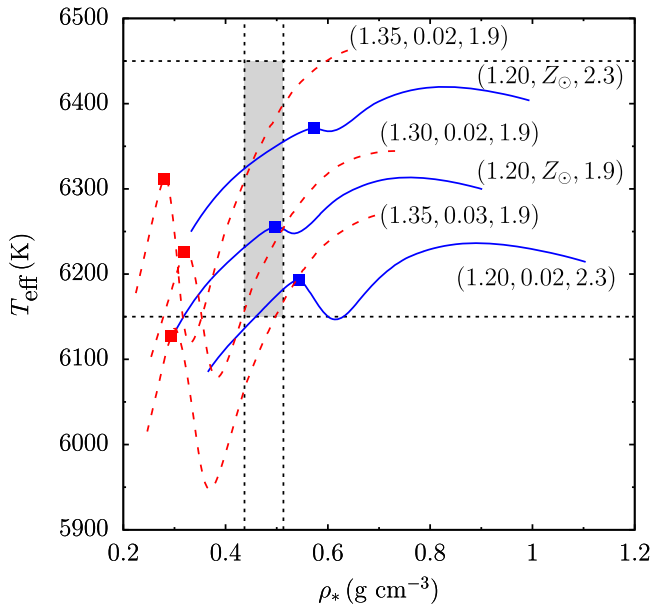


Figure 1. Evolution of the effective temperature T_{eff} and mean density ρ_* for six stellar models. Each model is labeled by $(M_*/M_\odot, Z, \alpha_{\text{MLT}})$. The evolution goes from right to left, starting from when the star is 1 Gyr old. The squares mark when the core ceases to be convective. Observations of WASP-12 constrain its T_{eff} and ρ_* to lie within the region indicated by the gray box. The blue solid (red dashed) curves are models that match the observations when on the subgiant branch (main sequence).

MESA prescriptions given in Choi et al. (2016) for calculating the abundances, equation of state, opacity, and reaction rates.

As we show below, the properties of WASP-12 are consistent with both $M_* \simeq 1.3 M_\odot$ main sequence models and $M_* \simeq 1.2 M_\odot$ subgiant models. The range of subgiant models that fits the observations is sensitive to how convection and mixing in radiative zones is implemented in MESA. In particular, we find it is sensitive to the values of the parameters of mixing length theory α_{MLT} , overshooting f_{ov} , semiconvection α_{sc} , and diffusive mixing. Although recent studies are starting to place interesting constraints on some of these parameters (Silva Aguirre et al. 2011; Magic et al. 2015; Moravveji et al. 2015, 2016; Deheuvels et al. 2016; Moore & Garaud 2016), there is still considerable uncertainty, especially as to how they depend on stellar mass, metallicity, and age. For simplicity, we therefore use the Schwarzschild criterion with $f_{\text{ov}} = 0$, we neglect diffusive mixing, and we consider a range of values for α_{MLT} .

In Figure 1 we show the evolution of T_{eff} and ρ_* for six stellar models. The three $M_* = 1.30$ – $1.35 M_\odot$ models (red dashed curves) match the observed constraints (gray box) when the star is on the main sequence. The three $M_* = 1.20 M_\odot$ models (blue solid curves) match the observed constraints during the post-main sequence phase, when the star is a subgiant and the core is no longer convective. The different models are selected in order to illustrate that the evolution of T_{eff} and ρ_* is sensitive to not only M_* , but also Z and α_{MLT} .

All six models shown in Figure 1 spend about 0.5 Gyr within the measured range of T_{eff} and ρ_* . During this portion of their evolution, the radii and surface gravity of the higher-mass models span $R_* = 1.50$ – $1.62 R_\odot$ and $\log g_* = 4.14$ – 4.20 , while the lower-mass models span $R_* = 1.47$ – $1.55 R_\odot$ and $\log g_* = 4.13$ – 4.18 . These are consistent with the (model-dependent) constraints reported in the literature.

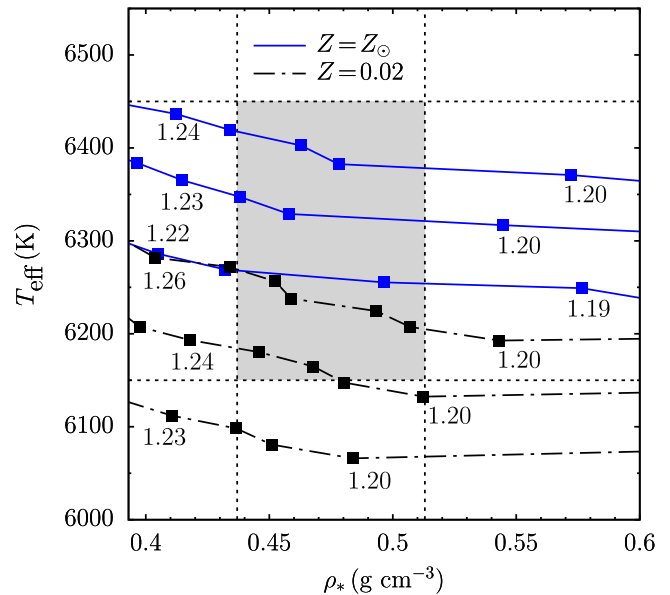


Figure 2. Effective temperature T_{eff} and mean density ρ_* at the moment when the core ceases to be convective and the star enters the subgiant phase. The labels indicate M_*/M_\odot with points spaced by $0.01 M_\odot$ (connected by straight lines for clarity). The blue solid curves assume solar metallicity $Z = Z_\odot = 0.0142$ and the black dashed-dotted curves assume $Z = 0.02$. The three curves for each Z assume, from bottom to top, $\alpha_{\text{MLT}} = 1.9, 2.1,$ and 2.3 . Observations of WASP-12 constrain its T_{eff} and ρ_* to lie within the region indicated by the gray box.

As we describe in Section 3, the efficiency of tidal dissipation is significantly enhanced if WASP-12 has a radiative core. The only models with radiative cores that we find are consistent with the measured T_{eff} and ρ_* are the subgiant models. Torres et al. (2012) estimate a somewhat lower $T_{\text{eff}} = 6118 \pm 64$ K, which could match the T_{eff} of main sequence models with fully radiative cores (i.e., $M_* \lesssim 1.1 M_\odot$). However, we find that such models have too high a ρ_* .

In Figure 2 we show T_{eff} as a function of ρ_* at the moment the core ceases to be convective and the star enters the subgiant phase. We find that for a given M_* , increasing α_{MLT} or decreasing Z increases T_{eff} and ρ_* . The models that are either inside or to the right (since ρ_* decreases with age) of the gray box are consistent with the observations for a portion of the subgiant branch. The constraints are consistent with subgiant models whose parameters lie in the range $1.20 \lesssim M_*/M_\odot \lesssim 1.25$, $Z_\odot \lesssim Z \lesssim 0.03$ (i.e., $0 \lesssim [\text{Fe}/\text{H}] \lesssim 0.3$), and $1.9 \lesssim \alpha_{\text{MLT}} \lesssim 2.3$.

3. Tidal Dissipation

The orbit of WASP-12 appears circular ($e < 0.05$; Husnoo et al. 2012), and given the age of the system, the planet's rotation is expected to be synchronized (Goldreich & Soter 1966; Rasio et al. 1996). Therefore, any ongoing tidal dissipation must be occurring within the non-synchronized host star. Dissipation mechanisms include turbulent damping of the equilibrium tide within the convective regions of the star and linear or nonlinear damping of the dynamical tide. Studies of the former find $Q_*' \sim 10^8$ – 10^9 (Penev & Sasselov 2011). This is more than three orders of magnitude too small a dissipation rate (too large a Q_*') to explain the apparent orbital decay of WASP-12. We therefore focus on tidal dissipation due to the dynamical tide.

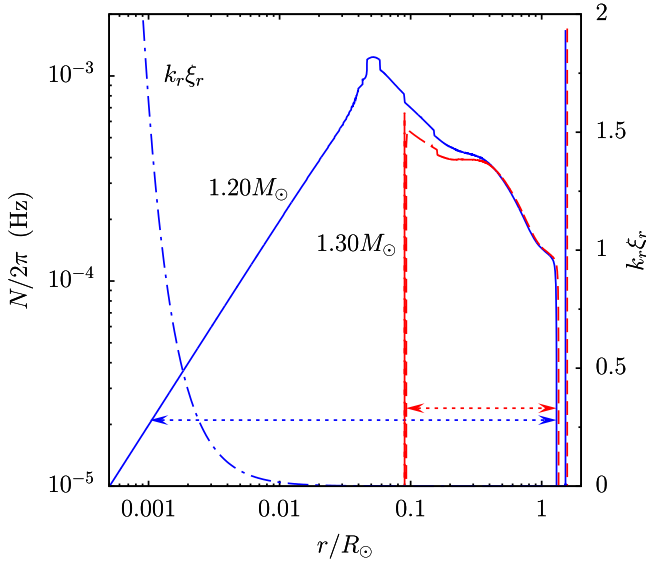


Figure 3. Radial profile of the Brunt-Väisälä frequency $N/2\pi$ (left axis) and the nonlinearity measure $k_r \xi_r$ (right axis). The blue solid curve and red dashed curve show $N/2\pi$ for two WASP-12 models, respectively: the subgiant model (M_*/M_\odot , Z , α_{MLT} , Age/Gyr) = (1.20, Z_\odot , 2.1, 3.7) and the main sequence model (1.30, 0.02, 1.9, 2.7). The blue dashed-dotted curve shows $k_r \xi_r$ for the subgiant model. The arrows indicate the turning points of the dynamical tide.

The dynamical tide in WASP-12 is dominated by resonantly excited internal gravity waves. Such waves propagate in the stratified regions of the star (where the Brunt-Väisälä buoyancy frequency $N^2 > 0$) and are evanescent within convective regions ($N^2 < 0$). As a result, the dynamical tide is excited near radiative-convective boundaries (RCBs), where its radial wavelength is long and it can couple well to the long length-scale tidal potential (Zahn 1975, 1977).

When a star like WASP-12 (a late-F star) is on the main sequence, it has both a convective core and a convective envelope. When core hydrogen-burning ends and the star evolves off the main sequence and becomes a subgiant, its core ceases to be convective. In Figure 3 we show N as a function of stellar radius r for a main sequence and subgiant model of WASP-12. In the main sequence model, the convective core extends from the center to $r \simeq 0.1 R_\odot$ and the convective envelope extends from $r \simeq 1.35 R_\odot$ to very near the surface. The propagation cavity of the dynamical tide is determined by these two radii (they are its inner and outer turning points, respectively; see the red arrows in Figure 3).

In the subgiant model, by contrast, $N^2 > 0$ all the way to the center. We find a linear scaling with radius $N \simeq Cr$ in the core, where $C \simeq 0.1(R_\odot \text{ s})^{-1}$. The dynamical tide propagates where the tidal frequency $\omega < N(r)$; for the dominant $\ell = 2$ tide, $\omega = 2\Omega$, where Ω is the orbital frequency. Thus, the tide raised by WASP-12b ($\omega/2\pi = 21.2 \mu\text{Hz}$) has an inner turning point at $r \simeq \omega/C \simeq 10^{-3} R_\odot$ during the subgiant phase (blue arrows in Figure 3). The dynamical tide propagates much closer to the center of the star when the star is a subgiant compared to when it is on the main sequence.

3.1. Dynamical Tide Luminosity and Wave-breaking

If the dynamical tide loses very little energy in the group travel time between turning points, it forms a global standing wave. Conversely, if it loses a significant fraction of its energy between turning points, it behaves more like a traveling wave

excited near the outer convection zone and traveling inward to the center. We will show that the dynamical tide is a standing wave for the main sequence models of WASP-12 and a traveling wave for the subgiant models. We now calculate the dynamical tide luminosity L assuming a traveling wave.

In the gravity wave propagation zone, the traveling wave luminosity is given by $L(r) = r^2 \int d\Omega \rho \psi_{\text{dyn}} \dot{\xi}_{r,\text{dyn}}$, where $\psi = \delta p / \rho + U$, δp is the Eulerian pressure perturbation, U is the tidal potential, ξ_r is the radial displacement, and the subscript “dyn” denotes the short-wavelength, dynamical tide piece. $L(r)$ is nearly constant with r in the propagation zone (except near sharp features such as density variations on short length scales³). To compute ξ_r and ψ , we solve the equations of motion of the linear tide (e.g., Weinberg et al. 2012). We use the Cowling approximation, in which the perturbed gravity is ignored, a good approximation for the short-wavelength dynamical tide. A mechanical boundary condition $\psi - U = g\xi_r$ is used at the surface of the star, and the inward-going traveling wave boundary condition $d(\psi - \psi_0)/dr = ik_r(\psi - \psi_0)$ is applied at a radius well within the propagation zone. Here, ψ_0 is an approximation of the long-wavelength, particular solution, called the “finite frequency equilibrium tide” (see Arras & Socrates 2010); it is given by $\Lambda^2 \psi_0 = \omega^2 d(r^2 \xi_{r,\text{eq}})/dr$, where $\Lambda^2 = \ell(\ell + 1)$ and $\xi_{r,\text{eq}} = -U/g$ is the radial displacement of the zero-frequency equilibrium tide. The dynamical tide piece of the solution is given by $\xi_{r,\text{dyn}} = \xi_r - \xi_{r,\text{eq}}$, and $\psi_{\text{dyn}} = \psi - \psi_0$.

This numerical calculation of L may be compared to analytic treatments in which approximate solutions in the radiative and convection zones are matched across the RCB (Zahn 1975; Goldreich & Nicholson 1989; Goodman & Dickson 1998; Kushnir et al. 2017). While an analytic treatment is, in principle, useful for providing simple formulae, the solution in the convection zone and the matching conditions at the RCB are complicated and can depend on ω and the size of the outer convection zone. Nonetheless, we derive an approximate fitting formula as follows. Given an equilibrium tide displacement $\xi_{r,\text{eq}} \simeq -U/g$, the dynamical tide near the RCB is $\xi_{r,\text{dyn}} \simeq \zeta (\lambda/r) \xi_{r,\text{eq}}$, where ζ is a dimensionless constant that depends on the structure of the convection zone found by the matching conditions, and $\lambda = [-\Lambda^2/\omega^2 r^2 dN^2/dr]^{-1/3}$ is the wavelength near the RCB. By the continuity equation, $\Lambda^2 \psi_{\text{dyn}}/\omega^2 r^2 \simeq d\xi_{r,\text{dyn}}/dr \simeq \xi_{r,\text{dyn}}/\lambda$. Thus, for the dominant $\ell = 2$ gravity wave,

$$L = A_L \frac{GM_p^2}{r_c} \left(\frac{r_c}{a}\right)^6 \left(\frac{\rho_c}{\bar{\rho}_c}\right) \left(\frac{\omega}{\omega_c}\right)^{8/3} \omega$$

$$\simeq 7 \times 10^{29} A_L \left(\frac{M_p}{10^{-3} M_*}\right)^2 \left(\frac{M_c}{M_\odot}\right)^{-7/3} \left(\frac{r_c}{R_\odot}\right)^{12}$$

$$\times \left(\frac{\rho_c}{10^{-3} \text{ g cm}^{-3}}\right) \left(\frac{P}{\text{day}}\right)^{-23/3} \text{ erg s}^{-1}, \quad (1)$$

where a is the semimajor axis, r_c is the radius of the RCB where the wave is excited, ρ_c is the density at r_c , $\bar{\rho}_c = 3M_c/4\pi r_c^3$ and M_c are the mean density and enclosed

³ Our stellar models have one or two sharp spikes in N (near $\sim 0.1 R_\odot$) due to composition discontinuities that form as the convective core shrinks. However, these spikes are unphysical; we find that they disappear when we include overshooting and diffusive mixing. Here, we simply smooth over them in order to calculate L .

mass within r_c , and $\omega_c = (GM_c/r_c^3)^{1/2}$ is the dynamical frequency at r_c . The dimensionless prefactor $A_L \approx 0.02\zeta^2[-(r_c/\omega_c^2)dN^2/dr]^{-1/3}$.

Equation (1) is similar to the form derived by Kushnir et al. (2017). It is useful if A_L is nearly constant for different P and stellar models. In practice, we find that this is not the case. Specifically, we find that for $P \lesssim 2$ days, A_L increases as P decreases (this is because at such large forcing frequencies, the wavelength is not sufficiently small compared to a scale height near the RCB; see Barker 2011). Furthermore, at a fixed $P = 1.1$ days, we find that the different WASP-12 subgiant models give values in the range $0.2 \lesssim A_L \lesssim 0.6$. Because of the complicated behavior of A_L , we rely on the numerical calculation of L rather than Equation (1).

If a fraction η of the wave luminosity L is deposited in a single group travel time across the star, then (Goldreich & Soter 1966; Ogilvie 2014)

$$\begin{aligned} \frac{P}{|\dot{P}|} &= \frac{G^{2/3}M_p M_* \Omega^{2/3}}{3(M_p + M_*)^{1/3} \eta L} \\ &\approx \frac{9.1}{\eta L_{30}} \left(\frac{M_*}{M_\odot} \right)^{2/3} \left(\frac{M_p}{M_{\text{Jup}}} \right) \left(\frac{P}{\text{day}} \right)^{-2/3} \text{ Myr}, \end{aligned} \quad (2)$$

where $L_{30} = L/10^{30} \text{ erg s}^{-1}$. The value of η depends on how efficiently the dynamical tide is dissipated as it propagates through the radiative interior.

The principal dissipation mechanisms acting on the dynamical tide are damping due to radiative diffusion and nonlinear wave interactions (Goodman & Dickson 1998; Barker & Ogilvie 2010; Weinberg et al. 2012; Essick & Weinberg 2016; Chernov et al. 2017). Radiative damping at a rate γ causes the amplitude of the tide to decrease by a factor of $\exp(-\gamma t_{\text{gr}})$ in a group travel time t_{gr} across the star. Damping due to nonlinear interactions is especially strong if the wave displacement ξ_r is so large that $k_r \xi_r \gtrsim 1$, where $k_r \approx \Delta N/\omega r$ is the radial wavenumber. Such a strongly nonlinear wave overturns the local stratification and breaks. Since it deposits all of its energy and angular momentum before reflecting, wave-breaking implies $\eta \approx 1$ (Barker & Ogilvie 2010; Barker 2011).

We can estimate $k_r \xi_r$ in the WKB approximation using conservation of energy flux, which states that $\rho N^2 v_{\text{gr}} |\xi_r|^2 \approx L/4\pi r^2$ as the dynamical tide propagates inward from the envelope RCB (Goodman & Dickson 1998). Here, $v_{\text{gr}} \approx \omega/k_r$ is the radial group velocity and ξ_r now denotes the rms radial displacement averaged over time and angles at fixed radius. This gives

$$\begin{aligned} k_r \xi_r &\approx \sqrt{\frac{\Lambda^3 N L}{4\pi \rho r^5 \omega^4}} \\ &\approx 1.3 \left(\frac{C_{0.1} L_{30}}{\rho_2} \right)^{1/2} \left(\frac{P}{\text{day}} \right)^2 \left(\frac{r}{10^{-3} R_\odot} \right)^{-2}. \end{aligned} \quad (3)$$

The second line represents the scaling in a radiative core, where $N = Cr$ with $C_{0.1} = C/0.1(R_\odot \text{ s})^{-1}$ and $\rho_2 = \rho/10^2 \text{ g cm}^{-3}$. Our numerical solutions of $k_r \xi_r$ agree well with this WKB estimate.

3.2. Resonance Locking

As a star evolves, its g -mode frequencies can increase, allowing them to sweep into resonance with the tidal

frequency. If the resulting tidal torques are sufficiently large, the dynamical tide can end up in a stable ‘‘resonance lock’’ and drive orbital decay on the stellar evolution timescale. Resonance-locking has been invoked to explain the observed properties of a variety of tidally interacting binaries (Witte & Savonije 2002; Fuller & Lai 2012; Burkart et al. 2013, 2014; Fuller et al. 2016, 2017).

We find that resonance-locking cannot explain the apparent orbital decay of WASP-12. This is because the g -mode frequencies in the models evolve too slowly for a mode to remain in resonance lock at the observed \dot{P} (even during the rapid evolutionary stage just before the convective core disappears). In the future, we plan to investigate whether resonance-locking is important in other short-period exoplanetary systems.

3.3. Tidal Dissipation on the Main Sequence

We find that tidal dissipation on the main sequence is too inefficient to explain the observed \dot{P} . Using the GYRE pulsation code (Townsend & Teitler 2013) to solve the non-adiabatic oscillation equations for the WASP-12 models, we find that $\gamma_{\text{gr}} \approx 10^{-6}$ for internal gravity waves resonant with the tidal forcing. Radiative damping is therefore an insignificant source of dissipation. This is consistent with the results of Chernov et al. (2017), who also consider radiative damping of the dynamical tide in main sequence models of WASP-12. Although they show that the observed \dot{P} could be explained if $\gamma_{\text{gr}} \sim 1$, which they refer to as the moderately large damping regime, they do not identify any mechanism that could enable the tide to be in this regime.

Furthermore, we find $k_r \xi_r \ll 1$ throughout the propagation cavity of the main sequence models. By Equation (3), $k_r \xi_r$ is largest near the inner turning point, which for the main sequence models is located at $r \approx 0.1 R_\odot$ (the top of the convective core); at this radius $k_r \xi_r \ll 1$. Thus, the dynamical tide does not break while the star is on the main sequence.

Even if $k_r \xi_r \ll 1$ and the dynamical tide forms a standing wave, it can still potentially lose energy through weakly nonlinear interactions involving three-mode couplings (Essick & Weinberg 2016). To check this, we computed three-mode coupling coefficients κ_{abc} using the methods described in Weinberg et al. (2012). We considered the stability of the dynamical tide to the resonant parametric instability, which involves the tide (mode a) coupling to daughter g -modes (modes b and c) whose eigenfrequencies satisfy $\omega_b + \omega_c \approx \omega_a$. We find that κ_{abc} is small ($\kappa_{abc} \sim 1$ using the normalization in Weinberg et al. 2012) and the tide is stable to the parametric instability (i.e., the nonlinear growth rate $\Gamma < \gamma$). We therefore conclude that while the star is on the main sequence, $\eta \ll 1$ and $P/|\dot{P}| \gg \text{Myr}$.

3.4. Tidal Dissipation on the Subgiant Branch

In the subgiant models, the radiative damping rate γ is again too small to significantly damp the dynamical tide. However, unlike the main sequence models, the subgiant models have a radiative core and a convective envelope. As a result, the inner turning point of the dynamical tide is much closer to the center of the star and we find that $k_r \xi_r \gtrsim 1$ near the inner turning point.

Our numerical solutions give luminosities in the range $L_{30} = [3.0, 10.5]$ for the subgiant models. Specifically, for the

subgiant model shown in Figure 3, we find $L_{30} = 3.6$. For this model, the key parameters of the convective envelope are $r_c \simeq 1.30 R_\odot$, $M_c \simeq 1.20 M_\odot$, $\rho_c \simeq 2.3 \times 10^{-3} \text{ g cm}^{-3}$, and the key parameters of the core are $\rho_2 \simeq 3.8$, and $C_{0.1} \simeq 1.3$. Plugging these into Equation (1) and taking $M_p = 1.40 M_{\text{Jup}}$ (Chan et al. 2011) gives $L_{30} \simeq 16A_L$, which, comparing to our numerical solution, implies $A_L \simeq 0.2$. Evaluating Equation (3) at the inner turning point $r = \omega/C = 1.0 \times 10^{-3} R_\odot$, gives $k_r \xi_r = 1.5$, in good agreement with the full numerical solution. Our other subgiant models yield very similar results, with values in the range $k_r \xi_r = [1.4, 2.5]$.

This implies that during the subgiant phase, the dynamical tide becomes strongly nonlinear near the inner turning point and breaks. As a result, $\eta \simeq 1$ and by Equation (2), the range in L implies decay timescales in the range $P/|\dot{P}| = [1.4, 4.5] \text{ Myr}$ (and $Q'_* = [0.8, 2.2] \times 10^5$). This agrees well with the observed $P/|\dot{P}| = 3.2 \pm 0.3 \text{ Myr}$.

Although we find $k_r \xi_r > 1$, it is only just slightly in excess of unity and one might wonder whether the wave really is efficiently damped ($\eta \simeq 1$). Numerical simulations by Barker (2011) show that as long as $k_r \xi_r > 1$, the wave breaks and efficiently transfers its angular momentum to the background mean flow. Furthermore, Essick & Weinberg (2016) find that if $k_r \xi_r \gtrsim 0.1$, the dissipation due to weakly nonlinear interactions with secondary waves is nearly as efficient as when $k_r \xi_r \gtrsim 1$. This therefore suggests that $\eta \simeq 1$ for the WASP-12 subgiant models.

4. Discussion

The main sequence and subgiant models are both $\approx 3 \text{ Gyr}$ old and spend $\approx 0.5 \text{ Gyr}$ within the measured range of T_{eff} and ρ_* . If the observed \dot{P} is indeed due to orbital decay, then an advantage of the subgiant scenario is that it naturally explains why the planet survived for 3 Gyr and is now decaying on a 3 Myr timescale. Although the system only spends $\sim 0.1\%$ of its life in the present state, there are $\simeq 30$ hot Jupiters with $P < 3 \text{ days}$ orbiting stars with $M_* > 1.2 M_\odot$. The dynamical tide likely breaks during the subgiant phase in these systems, thus they spend $\sim 0.1\%$ of their $\sim \text{Gyr}$ long lives in a state during which the planet decays on $\sim \text{Myr}$ timescales.⁴ We therefore estimate that out of the 30 systems, the probability of detecting one in a state like WASP-12 is $\sim 3\%$.

Even though wave-breaking of the dynamical tide can drive orbital decay on Myr timescales, it cannot spin up and align the entire star. This is because the wave breaks very close to the stellar center ($r < 0.01 R_\odot$), and while the torque L/Ω might spin up the stellar core (Barker & Ogilvie 2010), it is too small to strongly affect the spin at the stellar surface. Therefore, our results do not conflict with the observed slow, misaligned rotation of WASP-12.




A combination of continued transit timing and occultation observations over the next few years should resolve whether the WASP-12 timing anomalies are due to orbital decay or apsidal precession (Patra et al. 2017). Since we find that the decay scenario is only plausible if the star is a subgiant, tighter constraints on the stellar parameters can also help provide resolution. Given stellar modeling uncertainties, better constraints on just T_{eff} and ρ_* might not be sufficient.

⁴ As an aside, we note that because $P/|\dot{P}|$ increases rapidly with P , this mechanism cannot explain the apparent deficit of giant planets orbiting subgiants with periods between 10 and 100 days discussed in Schlaufman & Winn (2013).

Asteroseismology offers a promising alternative. Asteroseismic studies have determined whether stars are subgiants by measuring the sizes of convective cores (Deheuvels et al. 2016) and measured the masses and radii of stars hosting planets to few percent accuracy (Huber et al. 2013).

We thank Kishore Patra and Josh Winn for useful conversations and the referee for comments that improved the paper. This work was supported by NASA grant NNX14AB40G.

ORCID iDs

Nevin N. Weinberg  <https://orcid.org/0000-0001-9194-2084>
Phil Arras  <https://orcid.org/0000-0001-5611-1349>
Reed Essick  <https://orcid.org/0000-0001-8196-9267>

References

- Albrecht, S., Winn, J. N., Johnson, J. A., et al. 2012, *ApJ*, 757, 18
Applegate, J. H. 1992, *ApJ*, 385, 621
Arras, P., & Socrates, A. 2010, *ApJ*, 714, 1
Asplund, M., Grevesse, N., Sauval, A. J., & Scott, P. 2009, *ARA&A*, 47, 481
Barker, A. J. 2011, *MNRAS*, 414, 1365
Barker, A. J., & Ogilvie, G. I. 2010, *MNRAS*, 404, 1849
Birkby, J. L., Cappelletta, M., Cruz, P., et al. 2014, *MNRAS*, 440, 1470
Burkart, J., Quataert, E., & Arras, P. 2014, *MNRAS*, 443, 2957
Burkart, J., Quataert, E., Arras, P., & Weinberg, N. N. 2013, *MNRAS*, 433, 332
Chan, T., Ingemyr, M., Winn, J. N., et al. 2011, *AJ*, 141, 179
Chernov, S. V., Ivanov, P. B., & Papaloizou, J. C. B. 2017, *MNRAS*, 470, 2054
Choi, J., Dotter, A., Conroy, C., et al. 2016, *ApJ*, 823, 102
Deheuvels, S., Brandão, I., Silva Aguirre, V., et al. 2016, *A&A*, 589, A93
Enoch, B., Collier Cameron, A., Parley, N. R., & Hebb, L. 2010, *A&A*, 516, A33
Essick, R., & Weinberg, N. N. 2016, *ApJ*, 816, 18
Fossati, L., Bagnulo, S., Elmasli, A., et al. 2010, *ApJ*, 720, 872
Fuller, J., Hambleton, K., Shporer, A., Isaacson, H., & Thompson, S. 2017, *MNRAS*, 472, L25
Fuller, J., & Lai, D. 2012, *MNRAS*, 420, 3126
Fuller, J., Luan, J., & Quataert, E. 2016, *MNRAS*, 458, 3867
Goldreich, P., & Nicholson, P. D. 1989, *ApJ*, 342, 1079
Goldreich, P., & Soter, S. 1966, *Icar*, 5, 375
Goodman, J., & Dickson, E. S. 1998, *ApJ*, 507, 938
Hansen, B. M. S. 2010, *ApJ*, 723, 285
Hebb, L., Collier-Cameron, A., Loeillet, B., et al. 2009, *ApJ*, 693, 1920
Huber, D., Chaplin, W. J., Christensen-Dalsgaard, J., et al. 2013, *ApJ*, 767, 127
Husnoo, N., Pont, F., Mazeh, T., et al. 2012, *MNRAS*, 422, 3151
Jackson, B., Barnes, R., & Greenberg, R. 2009, *ApJ*, 698, 1357
Jackson, B., Greenberg, R., & Barnes, R. 2008, *ApJ*, 678, 1396
Kushnir, D., Zaldarriaga, M., Kollmeier, J. A., & Waldman, R. 2017, *MNRAS*, 467, 2146
Maciejewski, G., Errmann, R., Raetz, S., et al. 2011, *A&A*, 528, A65
Maciejewski, G., Dimitrov, D., Fernández, M., et al. 2016, *A&A*, 588, L6
Magic, Z., Weiss, A., & Asplund, M. 2015, *A&A*, 573, A89
Moore, K., & Garaud, P. 2016, *ApJ*, 817, 54
Moravveji, E., Aerts, C., Pápics, P. I., Triana, S. A., & Vandoren, B. 2015, *A&A*, 580, A27
Moravveji, E., Townsend, R. H. D., Aerts, C., & Mathis, S. 2016, *ApJ*, 823, 130
Ogilvie, G. I. 2014, *ARA&A*, 52, 171
Patra, K. C., Winn, J. N., Holman, M. J., et al. 2017, *AJ*, 154, 4
Paxton, B., Bildsten, L., & Dotter, A. 2011, *ApJS*, 192, 3
Paxton, B., Cantiello, M., Arras, P., et al. 2013, *ApJS*, 208, 4
Paxton, B., Marchant, P., Schwab, J., et al. 2015, *ApJS*, 220, 15
Penev, K., Jackson, B., Spada, F., & Thom, N. 2012, *ApJ*, 751, 96
Penev, K., & Sasselov, D. 2011, *ApJ*, 731, 67
Phinney, E. S. 1992, *RSPTA*, 341, 39
Rasio, F. A., Tout, C. A., Lubow, S. H., & Livio, M. 1996, *ApJ*, 470, 1187
Schlaufman, K. C. 2010, *ApJ*, 719, 602
Schlaufman, K. C., & Winn, J. N. 2013, *ApJ*, 772, 143
Seager, S., & Mallén-Ornelas, G. 2003, *ApJ*, 585, 1038

Silva Aguirre, V., Ballot, J., Serenelli, A. M., & Weiss, A. 2011, [A&A](#), [529](#), [A63](#)
Teitler, S., & Königl, A. 2014, [ApJ](#), [786](#), [139](#)
Torres, G., Fischer, D. A., Sozzetti, A., et al. 2012, [ApJ](#), [757](#), [161](#)
Townsend, R. H. D., & Teitler, S. A. 2013, [MNRAS](#), [435](#), [3406](#)

Watson, C. A., & Marsh, T. R. 2010, [MNRAS](#), [405](#), [2037](#)
Weinberg, N. N., Arras, P., Quataert, E., & Burkart, J. 2012, [ApJ](#), [751](#), [136](#)
Witte, M. G., & Savonije, G. J. 2002, [A&A](#), [386](#), [222](#)
Zahn, J.-P. 1975, [A&A](#), [41](#), [329](#)
Zahn, J.-P. 1977, [A&A](#), [57](#), [383](#)